Penerbit Akademia Baru

CFD Letters

Journal homepage: www.akademiabaru.com/cfdl.html
ISSN: 2180-1363

Comparison Between 6-DOF UDF and Moving Mesh Approaches in CFD Methods for Predicting Cross-Flow Pico-Hydro Turbine Performance

Open Access

Aji Putro Prakoso[1], Warjito[1*], Ahmad Indra Siswantara[1], Budiarso[1], Dendy Adanta[1]

[1] Mechanical Engineering Department, Faculty of Engineering, Universitas Indonesia

ARTICLE INFO

Article history:
Received 9 May 2019
Received in revised form 29 June 2019
Accepted 1 July 2019
Available online 3 July 2019

ABSTRACT

Many studies have been conducted on improving the performance of small-scale (micro-hydro and pico-hydro) cross-flow turbines using computational fluid dynamics (CFD) methods. In parallel with the development of technology, CFD methods are becoming increasingly sophisticated and are getting closer to real conditions in the field, with various developing features, progressing from the steady-state, transients with moving references, and moving mesh approaches, to using user-defined functions (UDF). This study compared the moving mesh method with the six degrees of freedom (6-DOF) UDF method for simulation of cross-flow turbines at the pico scale. The two simulations were treated as similarly as possible, outside of the dynamic approach, and were run in the 2D domain with 9.5 m of inlet head, using shear stress transport turbulence modelling. 6-DOF was found to have a much smaller deviation from experimental results, of about 6.8%, than the moving mesh results, at about 12.4% deviation. The deviation in the moving mesh results was assessed to be mainly caused by overcalculated turbulence conditions inside the rotating domain in the moving mesh calculation. The overcalculated turbulence condition makes the prediction of second stage energy absorption too low. The 6-DOF method is therefore more accurate than the moving mesh method for predicting the performance of cross-flow turbines at the pico scale. However, the moving mesh method is still an alternative because it has some advantages in terms of effectiveness of resource usage and rate of convergence.

Keywords:
Numerical simulation; Moving mesh; 6 DOF; Pico-hydro; Cross-flow

1. Introduction

Some regions in Indonesia do not yet have access to the national electricity grid and are categorised as remote areas [1]. Various studies have agreed that the best solution for providing electricity access in remote areas is to use an off-grid electricity network [2]. Off-grid electricity networks are independent micro-electricity networks that are separate from the centralised electricity network system. For electricity sources, micro-hydro and pico-hydro small-scale power plants are considered better than propellers and Pelton turbines, especially for areas that have high

* *Corresponding author.*
E-mail address: warjito@eng.ui.ac.id (Warjito)

rainfall levels [2,3]. One type of water turbine that is appropriate for use in a power plant in a remote area is a cross-flow turbine, with several advantages in simplicity and performance [4-6].

Many studies have been conducted on improving the performance of small-scale (micro-hydro and pico-hydro) cross-flow turbines using various methods, one of which is the computational fluid dynamics method. The CFD method is an approach to solving various fluid dynamics–related problems using numerical computation [7]. In parallel with the development of technology, CFD methods are becoming increasingly sophisticated and are getting closer to real conditions in the field, with various developing features, progressing from the steady-state, transients with moving references, and moving mesh approaches, to using user-defined functions (UDF). A UDF is a method in which certain functions are manually entered into CFD software and are then processed by that software [8].

Previous studies on small-scale cross-flow turbines using the CFD method have preferred either moving mesh or moving reference methods [9-12]. This is because those methods are sufficient to represent the actual conditions and are simpler than using UDFs; several such studies will be elaborated upon. Kaniecki and Staller [13] used CFD analysis to investigate the effect of draft tube additions to cross-flow turbines, using Fluent 5.0 in the 2D domain, with a moving reference frame method. Andrade *et al.,* [10] investigated the internal flow velocity and pressure field inside a cross-flow turbine runner and nozzle using CFD simulations in 2011, conducting a 3D simulation using ANSYS™ CFX 11® with a steady-state moving reference method. The root mean square (RMS) errors between the numerical simulations and the experimental test results in those studies were 5.37% and 7.99%, respectively. Sammartano *et al.,* [9] used CFD simulations to optimise some parameters that were discussed in their paper. The CFD procedure they ran used ANSYS™ CFX 13® in the 3D domain with a rotor–stator transient option; the optimum results were then tested in several experimental studies [14,15] to confirm design performance. The RMS error in Sammartano's study [14,15] was 4%. Elbatran *et al.,* [11] conducted CFD simulations and experimental tests to investigate the performance of their novel turbine configuration. Their study used ANSYS™ CFX® with unsteady analysis. Adhikari and Wood [12] used CFD analysis to examine their new cross-flow turbine nozzle design. In their study, the numerical simulation used ANSYS™ CFX® with a 3D domain; however, the dynamic approach in the study was not clearly explained.

In 2017, the ANSYS Fluent software offered an interface feature for a six degrees of freedom (6-DOF) UDF. With a 6-DOF UDF, an object can move automatically because of the interaction between the object and the surrounding fluid [8]. Several recent studies [5,6,16] have used this new feature because it is expected to be closer to the actual conditions of a turbine. Adanta *et al.,* [16,5], in 2018, used CFD simulations to determine the effect of cross-flow turbine blade curve depth on blade performance and investigate the reaction turbine effect in cross-flow turbines using air foil profiles in the blade, testing it using 2D ANSYS™ Fluent 18.2® with a 6-DOF UDF dynamics scheme. The experimental data in the study was then compared to data from Sammartano's study [14,15], finding an error in its numerical results of 1.9%. Siswantara *et al.,* [6] also assessed several types of turbulence model to identify a suitable one for cross-flow numerical simulations. The simulation was run using ANSYS™ Fluent 18.2® with a 2D domain and a 6-DOF UDF. The error calculated in the study was 1.5%. Using the same software and dynamic scheme, Adanta *et al.,* [17] also investigated the kinetic energy and bucket shape effect on breastshot waterwheel performance.

Although the 6-DOF feature in ANSYS™ Fluent 18.2® has been used for two years, there are no studies that compare 6-DOF with moving mesh methods. This study will compare the results of numerical simulations from a moving mesh and a 6-DOF method. The most noticeable difference between these two methods is how a turbine rotates. Moving mesh methods work by pegging the rpm of the turbine consistently, while the 6-DOF UDF rpm turbine method depends on the interaction

between the water and the runner. The results of this study should provide a recommendation as to which method is appropriate for simulating cross-flow turbines using ANSYS™ Fluent 18.2®.

2. CFD Simulation Procedure

2.1 Case Definition

To simplify the secondary data extraction process, this study used a duplication of Sammartano's [15], built as similarly as possible to the native case in the 2D domain. Table 1 is a design specification and Figure 1 is a representation of Table 1, or a schematic of geometry of the cross-flow turbine; more information can be found in previous studies [5,6].

Table 1
Cross-flow turbine parameters [15]

Design parameter	Value
Outer diameter (D)	161 mm
Inner diameter (d)	121 mm
Angle of attack (α)	22°
Number of blades	35
Blade inlet angle (β_1)	39°
Blade outlet angle (β_2)	90°
Blade curve radius (R_S)	22.5 mm
Blade curve angle (ϑ_S)	59°
Nozzle discharge angle (λ)	90°
Nozzle initial height (S_0)	47 mm

2.2 Boundary Condition

Based on previous studies, the inlet and outlet for the cross-flow turbine simulation were better defined as a pressure inlet and outlet, to enforce the limitations of the total and static pressures caused by the available head [4,6,16]. This is because a velocity inlet will cause overpressure when the turbine starts to rotate in the 6-DOF UDF simulation. The total pressure (P_{tot}) [Pa], defined in the inlet, is calculated by Eq. (1):

$$P\_tot = \gamma H \tag{1}$$

Here, γ is water-specific weight (9,810 N/m^3) and H is head (9.5 m). The turbulence intermittency for the inlet was 1, the intensity was 5%, and its viscous ratio was 10. This specification was the default specification of the inlet, and the total pressure in the outlet was defined as zero. Zero total pressure in the outlet indicates no further potential energy after passing the system, which means it is all converted into turbine mechanical energy, and the energy loss is composed of fluid kinetic energy, fluid pressure and thermal energy. The turbulence specification of the outlet was also the default as specified for the inlet.

This case was composed of two domains connected by the interface around the turbine runner. The first domain was defined as a rotating domain, including the turbine runner blades and the space inside the runner. The other, surrounding the rotating domain, was defined as a static domain consisting of the turbine nozzle and casing. The interface boundary condition was defined to let the fluid pass through this type of boundary; if the interfaces were not defined, Fluent would automatically interpret this as a wall, and the fluid from the inlet could not flow into the turbine runner.

All of the wall boundaries were specified with 0 mm of roughness height and a 0.5 roughness constant. There were two different treatments for the wall boundary of the blades, adjusted according to the dynamics approach. The adjustment for each approach is explained after the simulation specification part of this paper. This study's case boundary location is shown in Figure 1.

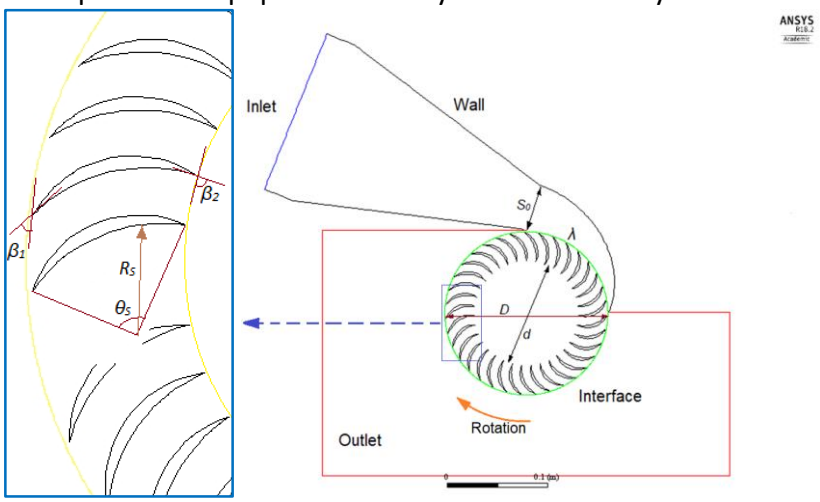

Fig. 1. Schematic of geometry and boundary location

The cross-flow turbine, which is an impulse turbine, is always working in the presence of air. Because of that condition, the multiphase modelling option was enabled in both cases. The specification of the multiphase modelling used the 'Volume of Fluid' model with implicit formulation and body force. The surface tension between the water and air was also defined as 0.0728 N/m [6,18].

To capture the turbulence flow, this study used the shear stress transport k-ω turbulence model [6,15,19] for both moving mesh and 6-DOF. The semi-implicit method for pressure-linked equations (SIMPLE) pressure–velocity coupling discretisation scheme was used for the calculations to make it more stable. For spatial discretisation, almost all magnitudes used a first-order upwind scheme, except gradient and pressure. The gradient discretisation used a least-square cell-based scheme and PRESTO discretisation scheme for pressure discretisation. The transient formulation used a first-order implicit scheme. The lowest order of discretisation was used to create a more stable calculation process, but it needed a finer mesh and timesteps to obtain accurate results. High-order term relaxation was also enabled for all variables.

2.3 Setup Specification of Six Degrees of Freedom

In the 6-DOF simulation, there were no settings for cell zone conditions, which was different to the moving mesh. Consequently, both domains (static and rotating) were not defined with any specific movement. The movement of the rotating domain was specified in the dynamic mesh setup; furthermore, the wall of the blade was allowed to remain static. The domain of rotation (including the blade) was defined as the rigid body in the dynamic mesh option. The blade boundary was specified as an active boundary and the remainder was specified as passive. The active condition meant that the boundary would interact with the fluid inside the domain, so only the blade condition was specified as active in this case.

The 6-DOF properties option 'One DOF Rotation' was enabled with 1 kg·m^2 moment of inertia. The moment of inertia was obtained from computer-aided design software mass-property simulation results. The preload constraint option was also enabled for the 6-DOF simulation and given as 1 N·m.

The preload option was enabled to prevent the turbine's impeller tip speed becoming higher than the water's tangential speed.

2.4 Setup Specification of Moving Mesh

For moving mesh, the rotating domain was defined as rotating at a constant speed in the cell zone condition option. In the boundary condition option, the turbine was also defined as rotating at the same speed. The rotational speed value for the cell zone and boundary conditions were set to vary across six different test cases. The six test cases were categorised as ratios of water tangential velocity to runner tangential velocity (V_T/U): 2.2, 2.0, 1.8, 1.6, 1.4 and 1.2. These conditions were based on verified and validated data [9]. The water tangential velocity (V_T) [Pa] was determined using Eq. (2):

$$V_T = C_v \cos(\alpha)\sqrt{2gH - \omega^2 R^2} \tag{2}$$

Here, C_v is the velocity coefficient (0.95), H is the available head [m], ω is the runner rotational speed [rad/s] and R is the radius of the runner [m].

2.5 Independency Test Method

The Richardson extrapolation method was used to estimate the exact value of tested variable that could vary due to increments in meshing fineness. To find the exact value of a variable, the convergence coefficient (p) should be determined. The value of p was calculated using an iteration method according to Eq. (3) [20].

$$p_{n+1} = \frac{\ln\left(\left(\frac{f_3 - f_2}{f_2 - f_1}(r_{12}{}^{p_n} - 1)\right) + r_{12}{}^{p_n}\right)}{\ln(r_{12} \cdot r_{23})} \tag{3}$$

Here, f_3, f_2 and f_1 are the variable values of the mesh – coarse, medium and fine, respectively; r_{12} and r_{23} are the ratios of the mesh numbers between fine and medium and between medium and coarse, respectively. An example determination of r is as follows:

$$r_{12} = \left(\frac{h_{fine}}{h_{medium}}\right)^{0.5} \tag{4}$$

Here, h_{fine} and h_{medium} are the element numbers in the fine and medium conditions, respectively. The next step is the determination of an exact value (f_0) or interpolation value in the infinite mesh conditions, which is estimated using Eq. (5) [20]:

$$f_0 = f_1 + \frac{f_1 - f_2}{r^p - 1} \tag{5}$$

The grid convergence index (GCI) is determined using Eq. (6) [20]:

$$GCI_{12} = 1.25 \left|\frac{1}{f_1}\frac{f_2 - f_1}{r^p - 1}\right| x100\% \tag{6}$$

For the timestep size independence test, the mesh independence test was adopted for a timestep case, and a different approach to the refinement ratio was used. The ratio for the timestep size independence is determined using

$$r_{12} = \frac{h_{fine}}{h_{medium}} \tag{7}$$

3. Results

3.1 Independence Test Results

The simulation for the mesh independence test was run using a steady-state approach for the sake of simplicity. Torque was used as data, which were then analysed using the GCI. There were four samples to be tested: 19k, 32k, 64k and 129k elements; the number of the mesh was then converted to a normalised grid spacing: 1, 1.41, 1.99 and 2.6, respectively.

Figure 2 is the mesh independence graphic using Richardson extrapolation analysis. From Figure 2, the result of the extrapolation for the exact value of torque (f_0) was 271.1 N·m. Based on this result and using Eq. (5), f_2, having an error from its f_0 of 2%. This means a mesh number of 64,450 elements could be used.

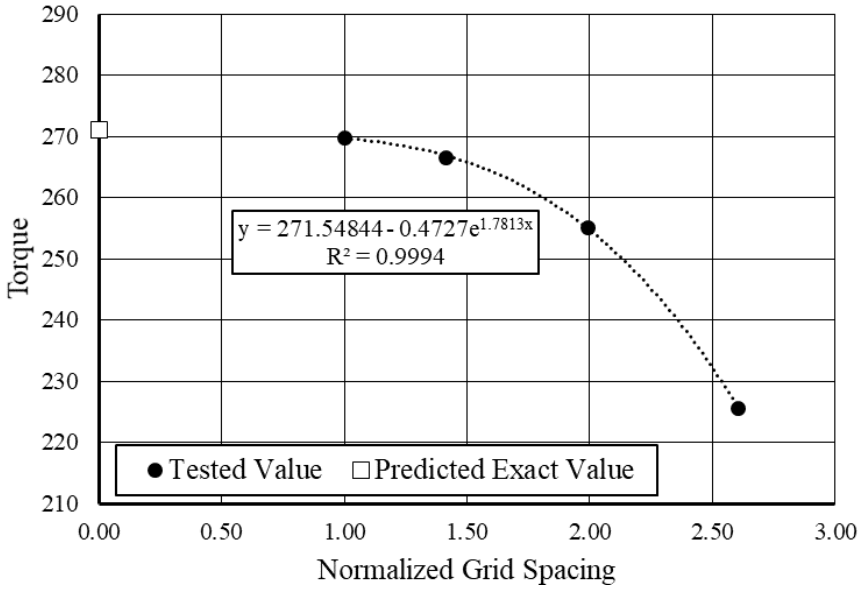

Fig. 2. Mesh independence test results

The mesh independence process, or GCI, was adopted to analyse the timestep independence test, called the convergence timestep index (CTI). The timestep independence process was used to test several sizes of timestep: 0.0002 s, 0.0004 s, 0.0008 s and 0.0064 s; the sizes of the timesteps were normalised to 1, 2, 4 and 8, respectively. Figure 3 shows the results of the extrapolation of the runner's torque with dynamics conditions of about 120.46 N·m. Based on the results in Figure 3, the CTI for f_2 for timesteps of size 0.0004 s had an error from its f_0 of 1%. This case was therefore used.

Figure 3 shows the timestep independence test results, with normalised timestep sizes from 1 to 8 for more focused discussion. Figure 3 also shows that the extrapolated dynamic runner's torque was about 120.46 Nm. The CTI – the adoption from CGI in the dynamic simulation at normalised timesteps of more than 4 – was still more than 5%. It was decided that the acceptance threshold for timestep independence would be 2% because, in timestep independence testing, the ratio of refinement in not rooted that should affect the acceptance threshold. In the condition with a

normalised timestep size of 4, the CGI was 2.2%; the CGI was then 1% at a timestep size of 0.0004 s. This case therefore used a mesh number of 64,450 elements and a timestep size of 0.0004 s. Figure 4 shows the mesh distribution.

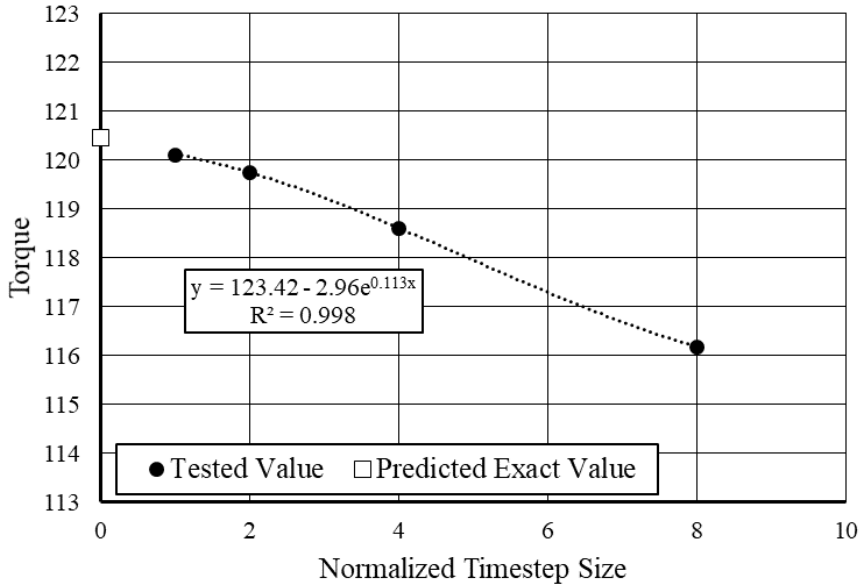

Fig. 3. Timestep independence test results

3.2 Turbine Simulation Comparison

The different results caused by different dynamic approaches are shown in Figure 5. The calculation results in Figure 5 show that the average deviation between the moving mesh approach and the experimental results was almost 12.4%, while the average deviation between the 6-DOF approach and the experimental results was about 6.8%. At the optimum condition, turbine performance calculation results were similar, as shown in Figure 6. Beyond that, larger deviations between the numerical and experimental data occurred at lower V_T/U (higher angular velocity condition), between 1.2 and 1.6. Conversely, smaller deviations occurred at a higher V_T/U of 2.2. The 6-DOF approach was much better than the moving mesh approach at predicting turbine performance.

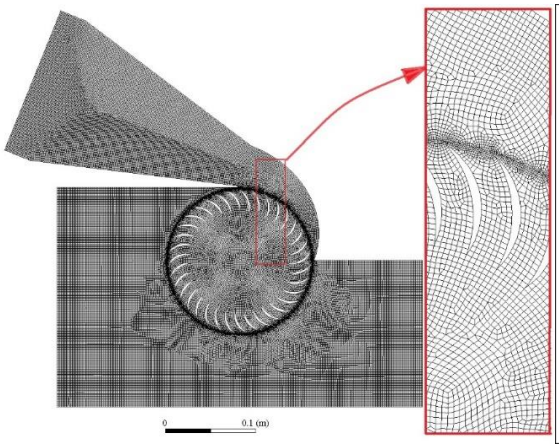

Fig. 4. Mesh distribution

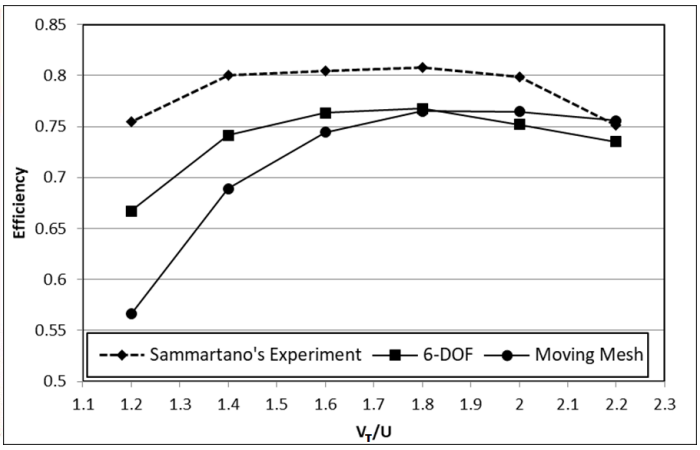

Fig. 5. Calculation results for 6-DOF and moving mesh

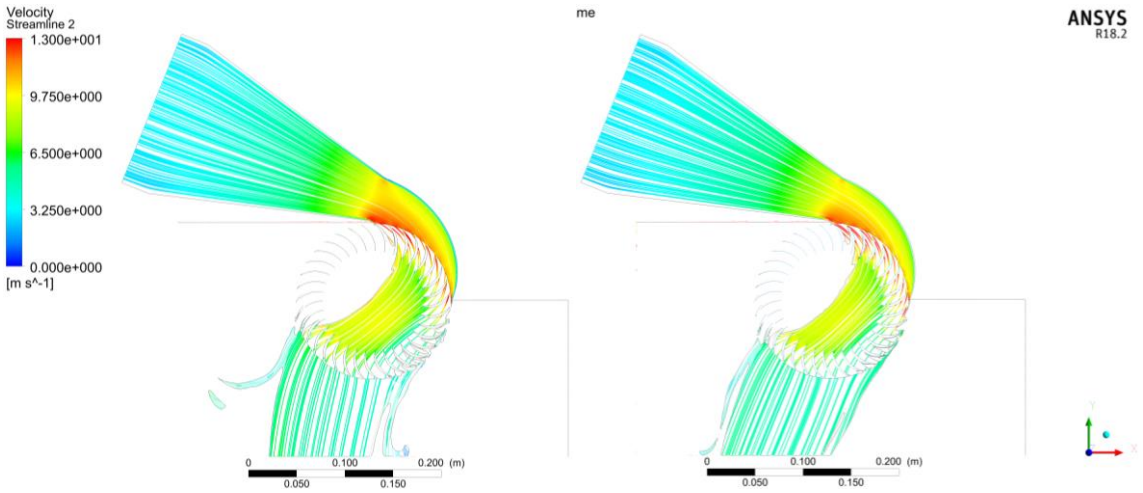

Fig. 6. Velocity streamline results at optimum condition: A. 6-DOF; B. Moving mesh

Figure 7 shows a comparison of the turbulence dissipation rate contour results from 6-DOF and moving mesh in the V_T/U of the 1.2 conditions. The deviation between the moving mesh approach and the experimental results appears to have been due to the moving rotor forcing the flow to dissipate so that the water power decreased. The overcalculation of the dissipation rate may also have caused the water velocity vector to change and decrease. The changed and decreased velocity vector of the water may have been because the domain was calculated as rotating with a specific angular velocity, while the water flow also has velocity. In this case, the average turbulence dissipation eddy inside the runner using 6-DOF was about 431 m^2/s^3, while the moving mesh calculation generated a value four times higher than the 6-DOF results, at about 1,631 m^2/s^3. The overcalculation of the turbulence dissipation rate indicates the overcalculation of turbulence that is characteristic of a cross-flow turbine, which also affected the total pressure drop when interacting with the turbine's blade in stage 2. The overcalculated turbulence characteristic resulted in overcalculation of the velocity randomness that occurs at the low energy harvest in stage 2. Figure 8 shows a comparison of the results of the total pressure contours of the 6-DOF and moving mesh simulations.

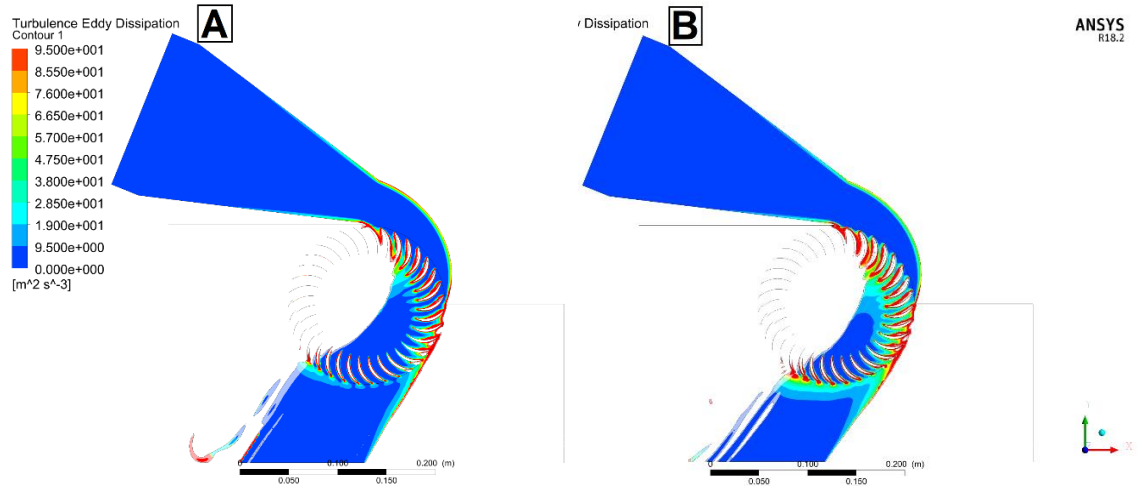

Fig. 7. Turbulence dissipation rate results at V_T/U of 1.2: A. 6-DOF; B. Moving mesh

With the same colour scaling, Figure 8 shows that the total water pressure when leaving the turbine in the moving mesh case was higher than in the 6-DOF case. This indicates that there was still some energy contained in the water that was not yet harvested in the moving mesh case. The energy

was harvested better in the 6-DOF case, as indicated by lower total water pressure when leaving the turbine. The overcalculated turbulence characteristic also occurred in the relative drag coefficient for water entering the turbine. This condition makes the water dynamic pressure when entering the turbine in the moving mesh case lower than in the 6-DOF condition, with the same static pressure. This phenomenon makes the water inlet mass flow in the moving mesh case lower than in the 6-DOF condition, as shown in Figure 9. It was also found that, at higher turbine angular velocity (lower V_T/U value), the deviation of the water inlet mass flow was greater. This condition was in line with above discussion.

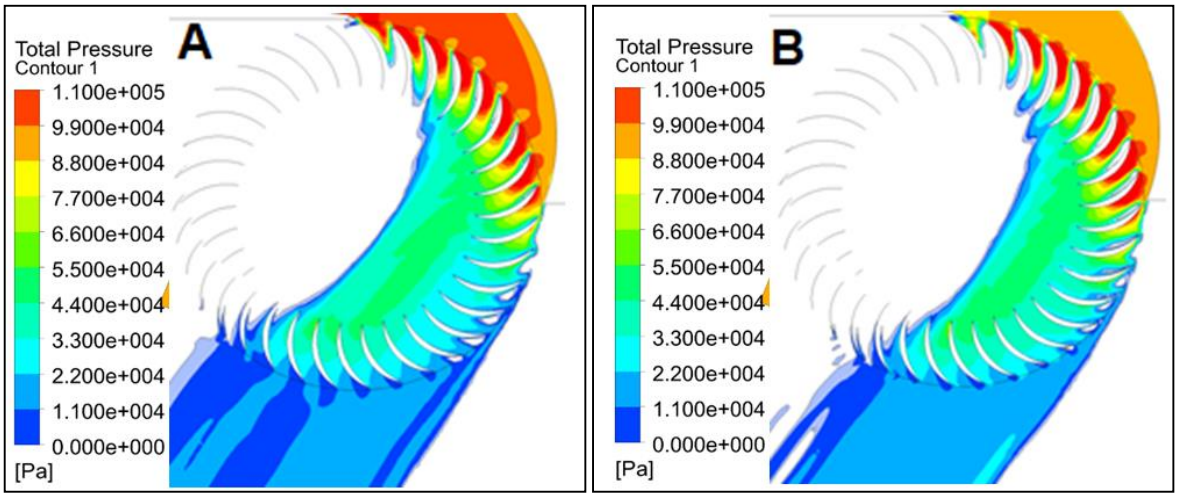

Fig. 8. Total pressure distribution contours at V_T/U =1.2: A. 6-DOF, B. Moving mesh

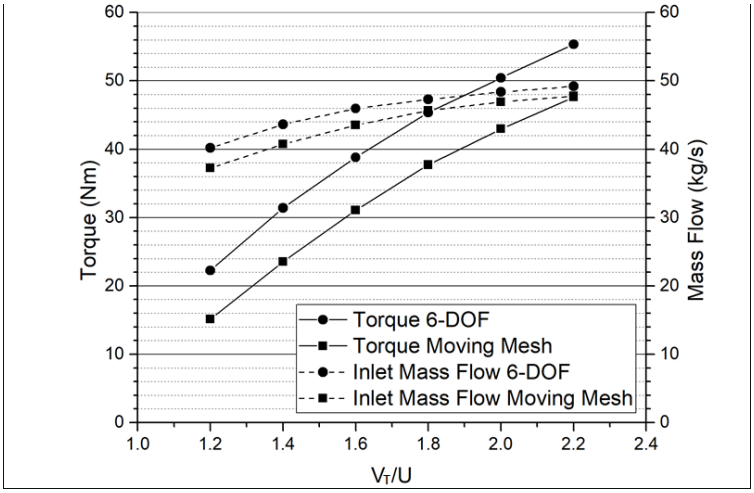

Fig. 9. Torque and mass flow results comparation between 6-DOF and Moving Mesh

The results above were in accordance with prior studies related to 6-DOF simulations [21-23]. Go *et al.,* [23] concluded that CFD simulations using 6-DOF can determine all linear and nonlinear hydrodynamic damping coefficients more accurately than other methods. Hopfe *et al.,* [21] also found that 6-DOF simulation methods can calculate significant aerodynamic forces and moments as well as other experimental calculations. Both of these studies showed that the 6-DOF UDF approach has better prediction results than other approaches in CFD numerical simulations. Kim et al. confirmed that 6-DOF calculations of all external forces for submarines are very accurate, with errors never greater than 8% [22].

Even though 6-DOF UDF simulations promise better prediction of pico-hydro cross-flow turbine performance, there are some technical points that mean that moving mesh simulations are still an option for cross-flow numerical simulation. In terms of resource usage, the simulation process using the 6-DOF approach used 2,000 timestep calculations to obtain the holistic data. It also needed five hours of computer time to finish the calculation. In contrast, the moving mesh simulation only required 250 timesteps for V_T/U variations, or a total of 1,500 timesteps, and needed less than three hours of computer time in a batch calculation. Because of the implicit statement of the turbine dynamics, it was more difficult for the 6-DOF simulation to reach convergence than the moving mesh simulation, for which the dynamics conditions of the turbine were stated before the calculation. However, the accuracy of the prediction in the 6-DOF condition was very promising, which is more significant than the other aspects.

4. Conclusions

This study found that 6-DOF has a much smaller deviation, of about 3.4%, from the experimental results than the moving mesh method, at about 10% deviation. The 6-DOF method is therefore more accurate than the moving mesh method for predicting the performance of cross-flow turbines at pico scale. However, the moving mesh condition has advantages in calculation time and rate of convergence.

Acknowledgement

This work was supported by the KEMENRISTEK DIKTI Republic of Indonesia with grant No: NKB-1777/UN2.R3.1/HKP.05.00/2019.

References

[1] P.T. PLN, Rencana Usaha Penyediaan Tenaga Listrik (RUPTL) 2015-2024, Jakarta PT PLN. (2015).
[2] Kaunda, Chiyembekezo S., Cuthbert Z. Kimambo, and Torbjorn K. Nielsen. "A technical discussion on microhydropower technology and its turbines." *Renewable and Sustainable Energy Reviews* 35 (2014): 445-459..
[3] W. Budiarso Dendy Adanta. "Kajian Turbin Air Piko Hidro Daerah Terpencil Di Indonesia." *Semin. Nas. Tah. Tek. Mesin XV* (2016) 5–7.
[4] Warjito, Ahmad Indra Siswantara, Dendy Adanta, Aji Putro Prakoso, Reza Dianofitra, Comparison Between Airfoil Profiled Blade and Ordinary Blade in Cross-Flow Turbine Using Numerical Simulation, in: 15th Int. Conf. Qual. Res., Faculty of Engineering, Universitas Indonesia, Bali, 2017.
[5] Adanta, Dendy, Warjito Budiarso, Ahmad Indra Siswantara, and Aji Putro Prakoso. "Performance comparison of NACA 6509 and 6712 on pico hydro type cross-flow turbine by numerical method." *Journal of Advanced Research in Fluid Mechanics and Thermal Sciences* 45, no. 1 (2018): 116-127.
[6] Ahmad Indra Siswantara, Budiarso, Aji Putro Prakoso, Gun Gun R Gunadi, Warjito, Dendy Adanta. "Assessment of Turbulence Model for Cross-Flow Pico Hydro Turbine Numerical Simulation." *CFD Letters* 10, no. 2 (2018) 38–48.
[7] H.K.H.K. Versteeg, W. Malalasekera, An introduction to computational fluid dynamics: the finite volume method, Pearson Education, 2007.
[8] ANSYS FLUENT UDF Manual, ANSYS, Inc, Canonsburg, PA, 2011.
[9] Sammartano, Vincenzo, Costanza Aricò, Armando Carravetta, Oreste Fecarotta, and Tullio Tucciarelli. "Banki-Michell optimal design by computational fluid dynamics testing and hydrodynamic analysis." *Energies* 6, no. 5 (2013): 2362-2385.
[10] De Andrade, Jesús, Christian Curiel, Frank Kenyery, Orlando Aguillón, Auristela Vásquez, and Miguel Asuaje. "Numerical investigation of the internal flow in a Banki turbine." *International Journal of Rotating Machinery* 2011 (2011).
[11] Elbatran, A. H., O. B. Yaakob, Yasser M. Ahmed, and Ahmed S. Shehata. "Numerical and experimental investigations on efficient design and performance of hydrokinetic Banki cross flow turbine for rural areas." *Ocean Engineering* 159 (2018): 437-456.
[12] Adhikari, R. C., and D. H. Wood. "A new nozzle design methodology for high efficiency crossflow hydro turbines." *Energy for Sustainable Development* 41 (2017): 139-148.

[13] Kaniecki, Maciej. "Modernization of the outflow system of cross-flow turbines." *Task Quarterly* 6, no. 4 (2002): 601-608.
[14] Sammartano, V., G. Morreale, M. Sinagra, A. Collura, and T. Tucciarelli. "Experimental study of cross-flow micro-turbines for aqueduct energy recovery." *Procedia Engineering* 89 (2014): 540-547.
[15] Sammartano, Vincenzo, Gabriele Morreale, Marco Sinagra, and Tullio Tucciarelli. "Numerical and experimental investigation of a cross-flow water turbine." *Journal of Hydraulic Research* 54, no. 3 (2016): 321-331.
[16] Adanta, Dendy, Richiditya Hindami, and Ahmad Indra Siswantara. "Blade Depth Investigation on Cross-flow Turbine by Numerical Method." In *2018 4th International Conference on Science and Technology (ICST)*, pp. 1-6. IEEE, 2018.
[17] PPS, Jonathan Sahat, Dendy Adanta, and Aji Putro Prakoso. "Influence of Bucket Shape and Kinetic Energy on Breastshot Waterwheel Performance." In *2018 4th International Conference on Science and Technology (ICST)*, pp. 1-6. IEEE, 2018.
[18] D. Adanta, A.P. Prakoso, A.I. Siswantara, Warjito, Budiarso, Simplification Design of Nozzle and Blade of Pico Hydro Turbine type Cross-flow, in: 17th Annu. Natl. Ceminar Mech. Eng. (SNTTM XVII), BKSTM, Kupang, 2018: pp. 212–217.
[19] Adanta, Dendy, Warjito Budiarso, and Ahmad Indra Siswantara. "Assessment of turbulence modelling for numerical simulations into pico hydro turbine." *Journal of Advanced Research in Fluid Mechanics and Thermal Sciences* 46, no. 1 (2018): 21-31.
[20] Richards, Shane A. "Completed Richardson extrapolation in space and time." *Communications in numerical methods in engineering* 13, no. 7 (1997): 573-582.
[21] Hopfe, Norman, Pedro Caldas-Pinto, and Guido Kurth. "Funnel Flight Controller for a TDR 6-DoF Simulation Model." *IFAC Proceedings Volumes* 46, no. 19 (2013): 125-130.
[22] Kim, Howan, Dev Ranmuthugala, Zhi Quan Leong, and Christopher Chin. "Six-DOF simulations of an underwater vehicle undergoing straight line and steady turning manoeuvres." *Ocean Engineering* 150 (2018): 102-112.
[23] Go, Gwangsoo, and Hyung Taek Ahn. "Hydrodynamic derivative determination based on CFD and motion simulation for a tow-fish." *Applied Ocean Research* 82 (2019): 191-209.